Patterned surfaces in the drying of films composed of water, polymer, and alcohol

Julie Fichot,[1,2] Rodolphe Heyd,[1] Christophe Josserand,[3,*] Igor Chourpa,[4] Emilie Gombart,[2]
Jean-Francois Tranchant,[2] and Marie-Louise Saboungi[1,5,†]

[1]*Centre de Recherche sur la Matière Divisée, CNRS, Université d'Orléans, France*
[2]*LVMH Recherche, 185 avenue de Verdun 45800 Saint Jean de Braye, France*
[3]*Institut D'Alembert, CNRS, UPMC (Université Paris VI), UMR 7190, 4, place Jussieu, Paris F-75005, France*
[4]*Groupe Nanovecteurs Magnétiques pour la Chimiothérapie, EA 6295 Nanomédicaments et Nanosondes, Université François Rabelais de Tours, 31 avenue Monge, Tours F-37200, France*
[5]*IMPMC-CNRS, Université Pierre et Marie Curie, Paris Cedex 05, 75252 France*

(Received 17 December 2011; revised manuscript received 23 October 2012; published 7 December 2012)

A study of the complex drying dynamics of polymeric mixtures with optical microscopy and gravimetric measurement is presented. Droplet formation is observed, followed by a collapse that leads to the residual craters in the dried film. The process is followed *in situ* under well-defined temperature and hygrometric conditions to determine the origin and nature of these droplets and craters. The drying process is usually completed within 1 h. The observations are explained using a simple diffusion model based on experimental results collected from mass and optical measurements as well as Raman confocal microspectrometry. Although the specific polymeric mixtures used here are of interest to the cosmetic industry, the general conclusions reached can apply to other polymeric aqueous solutions with applications to commercial and artistic painting.

DOI: 10.1103/PhysRevE.86.061601 PACS number(s): 68.03.Fg, 82.40.Ck, 47.20.Hw

I. INTRODUCTION

The drying of complex fluids is a subject of considerable current interest from a fundamental perspective in addition to its involvement in applications ranging from commercial and artistic painting and inkjet printing to the food and cosmetic industries [1–10]. The drying kinetics involves different physical mechanisms, such as diffusion, convection, Marangoni effects, and contact line motion. When particles are in suspension in the liquid, for instance, during drop evaporation, the pinning of the contact line leads to convective motions within the drop, which can produce film deposition similar to that observed in coffee rings [2,11,12]. Alternatively, a moving contact line can dominate the evaporation dynamics, for instance, in the case of polymer film evaporation on a nonwettable substrate [13,14] or along a meniscus [15]. In many cases, however, the dynamics can give rise to the formation of regular patterns as observed in colloidal gels due to buckling-driven delamination [16] in block polymer self-assembly processes [17] and in polymer films due to phase separation [18,19] or thermocapillary convection [20]. In cosmetics, films with thicknesses varying from 10 μm to 1 mm are usually spread on human skin and are, consequently, subject to strong evaporation rates due to temperature gradient and dryness. Therefore, an investigation of the *in situ* evolution of some key properties, such as elasticity, texture, viscosity, or porosity would be of great importance. Here, we report results of combined experiments and modeling to provide a description of the *in situ* evolution of the drying of a relatively thin film ($\sim$100 μm) deposited on a substrate under controlled environmental conditions.

II. EXPERIMENTS

A simple fluid with the principal chemical and physical features of typical cosmetic films was selected, consisting of an aqueous solution of a polymer—sodium carboxymethylcellulose (NaCMC)—at an initial mass fraction of 3% together with a small quantity of a preservative agent, 2-phenoxyethanol $C_8H_{10}O_2$ (XOH), partially miscible in pure water up to a 2.4% mass fraction at 20 °C under experimental conditions. The initial mass fraction of XOH was always taken below the miscibility limit. The XOH has an aromatic ring due to an ether function connected to an OH group and has very little affinity with the CMC. The role of this preservative agent is crucial in the cosmetic context since it avoids the proliferation of micro-organisms in the fluid. The formulation prepared at 80 °C was stirred for 60 min with a magnetic agitator. After cooling it down to well-defined experimental conditions [$T = 20 \pm 2$ °C, relative humidity (RH) $= 42 \pm 5$%, fixed for all subsequent experiments], a drop of this mixture is spread onto either a polymethylmethacrylate (PMMA) or a G200 glass substrate (surface area $S = 15 \times 10$ cm^2) using a manual spreader made of a horizontal squeegee. This spreading method was selected to allow the best reproduction of the application of a cosmetic product on the skin yielding a film thickness of 85 ± 25 μm and a 3 μm typical roughness. The substrate covered with the film is then positioned on a balance, all these operations being performed *in situ* under controlled environmental conditions. The initial time $t = 0$ is defined at the end of this deposition process. Continuous snapshots of the films taken during the evaporation process (Fig. 1) showed the appearance of about 5 μm diameter small droplets after 18 min [Figs. 1(a) and 1(c)], which grow and coalesce into larger drops [Fig. 1(d)]. At the end of the drying process, the film is at equilibrium with the ambient environment, and no further evolution is observed. The droplets lead to the formation of about 4 to 5 μm diameter craters resulting probably from the polymer deficit in these droplets [Figs. 1(b)

*christophe.josserand@upmc.fr
†ml.saboungi@gmail.com

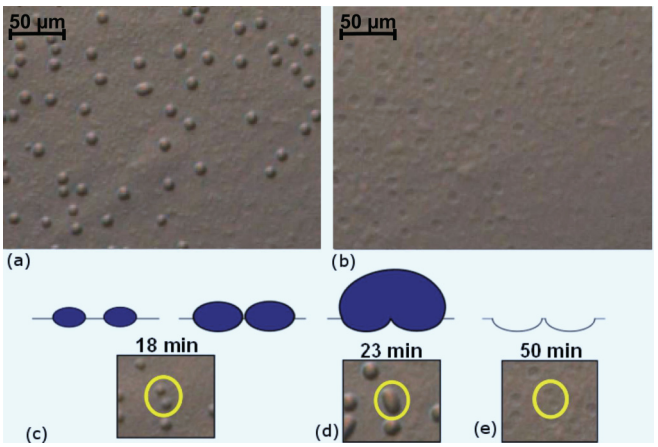

FIG. 1. (Color online) Typical binocular microscope images of the films during drying on a G200 glass substrate: (a) Surface of the film center when droplets appear at $t = 18$ min; (b) final dried film at $t = 50$ min with craters left by the droplets. The three snapshots (c)–(e) at the bottom show a closeup (illustrated schematically above) of the drying region that exhibits a coalescence of two droplets between $t = 18$ and $t = 23$ min, respectively, and the final craters with the trace of the two initial droplets.

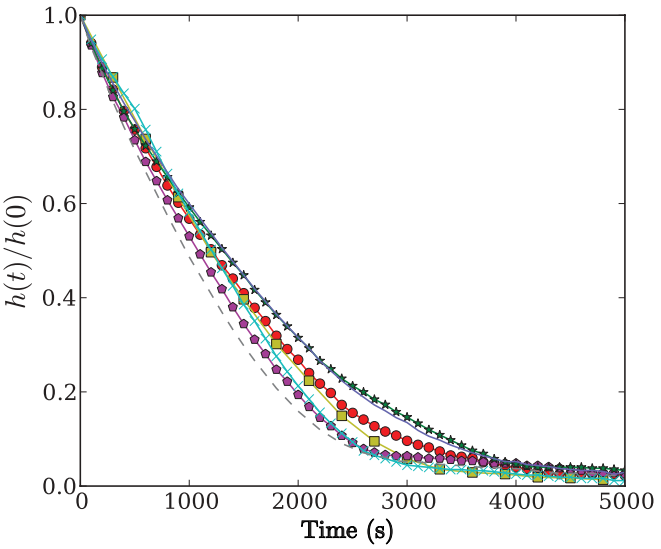

FIG. 2. (Color online) Evolution with time of the relative film height $h(t)/h(0)$ for an aqueous film made with a 3% initial mass fraction of polymer and with different XOH initial mass fractions red (circle): $w_{\mathrm{XOH}} = 0.4$; yellow (square): 0.6; magenta (pentagon): 0.8; green (star): 1.0; cyan (cross): 1.2; blue (continuous line): 1.8; and black (dashed line): 2.4%. The relative humidity and temperature are fixed at $42 \pm 5\%$ and $20 \pm 2\,^{\circ}$C, respectively.

and 1(e)]. Because of the low saturated vapor pressure (4 Pa) of XOH, we assumed, to a good approximation, that only water evaporates in the time range of these experiments.

The thickness and the composition of the initial films are not perfectly homogeneous due to both the preparation of the formulation and the spreading mechanism. Since the viscosity of the mixture is initially very high, 325 Pa s^{-1} (about 3×10^5 that of water, measured with a Kinexus viscometer) due to the polymer and increases even further during the evaporation, there is no convection within the film as supported by the persistence of the craters in the dried films [21,22].

Replacing NaCMC by sodium alginate does not affect the results, but the XOH removal leads to the disappearance of the droplets and, thus, of the craters. However, droplets are present when the solution contains only XOH without any polymer, but no craters are observed in this case. These observations illustrate that: (a) the presence of XOH is crucial for droplet formation, and (b) the polymer is needed for the drying of droplets into craters. Therefore, in order to disentangle the different roles played by the two components in the drying process, we have carried out gravimetric, Raman, and optical measurements.

We first followed the time evolution of the film thickness by measuring the film mass $m(t)$ using a high-precision balance (Kern with 0.0001 g precision). Because of the film dimensions, the evaporation process can be reduced to a one-dimensional (1D) problem with the film bounded by the substrate at $z = 0$ and the air interface at $z = h(t)$. The film height is deduced from the film mass using the initial mixture mass density ρ and is given by $h(t) = m(t)/S/\rho$: In fact, the exact meaning of this effective height is the height that would have a film of the same mass composed of the initial mixture. Due to the spreading mechanism, the initial film thickness is found to vary slightly between the experiments [$h(0) = 85 \pm 25$ μm]. Figure 2 shows the evolution of the relative height $h(t)/h(0)$ of the film for different initial mass fractions of XOH, w_{XOH}, but constant initial polymer mass fraction, RH, and T.

For all initial values of w_{XOH}, we observe a similar behavior consisting of an initial linear decrease in the height followed by a slowing down towards the final thickness. As the thickness decreases, the mass fractions of the polymer and of XOH increase so that water evaporation becomes more difficult due to the decreasing of the water content and, consequently, of the water activity at the moving interface, leading to the lowering of the water diffusion through the polymer matrix [23]. Finally, the film height reaches an asymptotic level where the water density inside the polymer matrix is at equilibrium with the imposed RH. Note that this level varies between experiments because of the variation in the thickness and the heterogeneity of the initial films.

Raman confocal microspectrometry experiments were used to follow the XOH distribution inside the film. As shown in Fig. 3, no detectable XOH peaks can be noticed during the drying process. On the other hand, once the film is dried, XOH is observed in the crater left by the droplet as presented in Fig. 4, demonstrating that the XOH concentrates somehow into the droplets. As the water evaporates, a phase separation in XOH concentration occurs because the XOH mass fraction becomes higher than the miscibility limit in some regions of the film. However, it raises the question of the detailed mechanism of this demixing transition: Does it create XOH droplets, or does it form a protective XOH thin shell around pure water droplets (the thickness of the XOH shell being small compared to the radius of the drop)? The not detectable Raman signal of XOH, as long as the water has not substantially evaporated, suggests that the latter scenario is the most consistent one.

To confirm that the formation of the droplets in the films is associated with a demixing transition, we prepared a binary

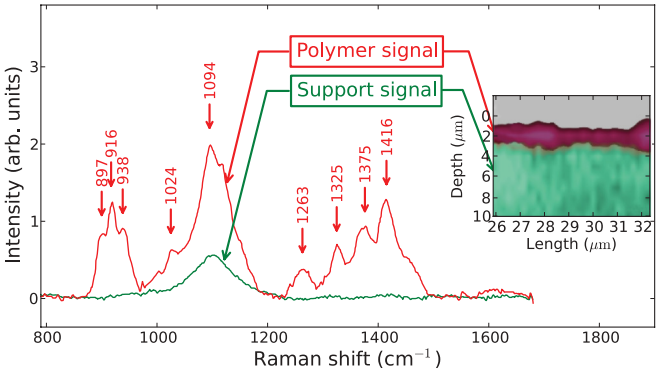

FIG. 3. (Color online) Confocal Raman microspectroscopy of a droplet: The Raman peaks are only those corresponding to top signal: the polymer and bottom signal: the substrate. Bottom of the picture: the confocal microspectroscopy image shows only the presence of the polymer above the substrate.

solution with only XOH and water in the same proportion as in the film with the polymer. A 0.2 μl drop of the solution was deposited on a PMMA substrate and was examined with an optical microscope during drying (Fig. 5). The results showed that droplets occur even when the polymer is not present. At first, tiny droplets appear near the contact line [Fig. 5(a)] where the solubility limit is quickly reached due to water evaporation, similar to what is observed in coffee rings [2,24–26]. As the drop dries, its diameter shrinks, leaving a ring-shaped XOH layer around it. Simultaneously, the droplets accumulate water by coalescence, enlarge, and concentrate most of the material of the drop [Fig. 5(b)], demonstrating that the XOH demixes into interfaces that form shells around pure water droplets. When the droplets reach a limiting diameter, the interfacial forces of their envelopes are not strong enough to balance the tension of the film, and they burst [27]. The water is freed and evaporates quickly leaving an oily XOH trace on the substrate. Indeed, since the saturated vapor pressure of XOH is low compared to that of water, it evaporates much slower: For instance, for the present volume, it takes about 10 min to

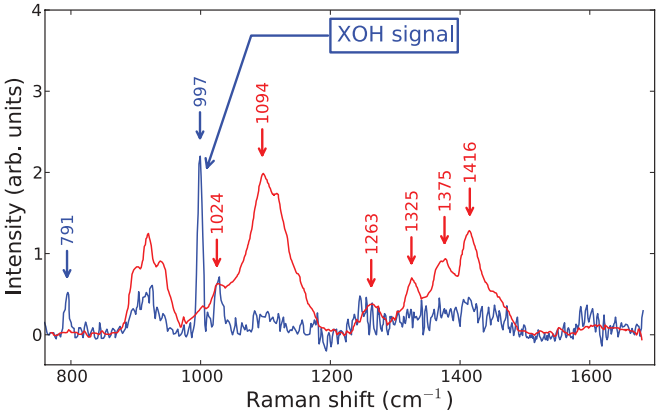

FIG. 4. (Color online) Raman microspectroscopy of the crater left after the drying of the same droplet analyzed in Fig. 3. In that case, the XOH signal is detected in the crater in addition to the polymer one. The substrate signal is not shown for clarity but is identical to that of Fig. 3.

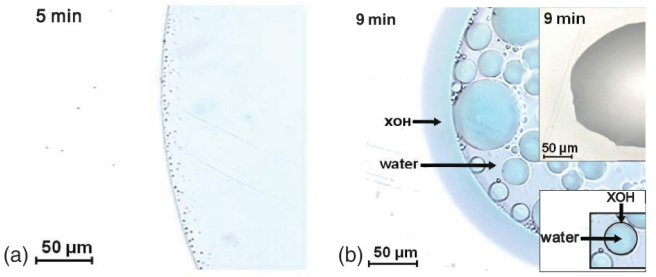

FIG. 5. (Color online) Optical microscope images of the drying of an XOH-water drop. (a) First droplets appear near the contact line; (b) coalescence of droplets and deposition of XOH around the droplets due to water evaporation. Upper inset: a pure water drop shows no droplet formation during evaporation. Lower inset: closeup showing the XOH shell around the water droplet.

evaporate the water and 60 min to evaporate the XOH. On a time scale of 10 min, XOH can, thus, be considered inert.

The same dynamics were observed for the water-polymer-XOH mixture, implying that the droplets were composed of pure water surrounded by an XOH shell as already suggested by the Raman microspectroscopy observations. Finally, drops of other mixtures containing water and other soluble materials were analyzed by optical microscopy during drying. Those with totally miscible constituents never form droplets, whereas, those with partially miscible constituents form either droplets (phenol and phenoxyisopropanol) or films (ethanol, 2-butanol, diphenyl ether, and di-isopropyl ether), depending on the wettability and viscosity of the constituents.

We, therefore, ascribe the droplet formation to the demixing of XOH that arises when its mass density exceeds the miscibility limit in water, i.e., when $w_{\mathrm{XOH}} > 0.024$. The evaporation consists of diffusion of molecules through the liquid-gas interface so that the saturated vapor pressure is the main parameter controlling the evaporation of each species. Since the saturated vapor pressure of XOH is much smaller than that of water, the drying kinetics is dominated first by the water evaporation followed much later by that of XOH so that the two processes can be separated.

III. NUMERICAL MODELS

The evaporation rate per surface area is a complex function that depends on the interface features, including interface temperature, humidity, and polymer and glycol ether mass fractions [28,29]. In general, such a function is hard to deduce when many parameters and large variations are present. Assuming a homogenous film, the evolution with time of the film thickness $h(t)$ can be written formally,

$$\dot{h} = \frac{dh}{dt} = \mathcal{F}[h(t), T, \mathrm{RH}, w_{\mathrm{XOH}}(h(t),t), w_{\mathrm{pol}}(h(t),t)], \quad (1)$$

where T is the temperature, RH is the relative humidity, and $w_{\mathrm{XOH}}(h(t),t)$ and $w_{\mathrm{pol}}(h(t),t)$ are the concentration *at the interface* of XOH and of the polymer, respectively. More complex effects accounting for a temperature jump at the interface could be considered but with no fundamental changes in the general formulation (1). It is important to note that, in our present case, we know this evaporation rate experimentally

since it can be directly extracted from the mass measurements shown in Fig. 2. From these curves, we can deduce that the evaporation rate depends weakly on w_{XOH}. Moreover, it is almost independent of the polymer concentration at least under the typical time scale of interest here, i.e., until the droplets appear. Clearly, in the latter times of the drying, the evaporation rate is lowered because the diffusion of the water molecule is affected by the dense polymer matrix. Finally, considering the constant environmental conditions (T and RH) of the experiments, the evaporation rate becomes a function of the film height only $\mathcal{F}(h(t))$. With this evaporation rate, we can compute the formation time of the droplets since they only appear when the w_{XOH} exceeds its miscibility limit at some location in the film. *A priori*, the concentration of XOH is not homogenous in the film, although the initial condition at $t = 0$ is homogenous, since the evaporation process increases the amount of XOH near the interface, whereas, diffusion tends to homogenize it within the film. We demonstrate, here, that we need to investigate this whole coupled dynamics (evaporation and XOH diffusion) to understand the droplet formation mechanism. Let us first assume that the diffusion of XOH in the film is fast so that, at any time, the mass fraction of XOH w_{XOH} is uniform. In other words, the diffusion coefficient of XOH in the mixture is sufficiently high to allow the full dilution of XOH in the film at each time. In this dilution regime, the concentration of XOH is constant in the film and is a function of time given by

$$w_{\mathrm{XOH}}(t) = \frac{h(0)}{h(t)} w_{\mathrm{XOH}}(0). \tag{2}$$

As shown in Fig. 6, this simple picture is in contradiction with the observations since the droplets appear much before the predicted time, suggesting that XOH diffusion within the film has to be considered as the water evaporates. Therefore, we account for the XOH concentration profiles for the film thickness evolution.

It follows that $w_{\mathrm{XOH}}(z,t)$ is now a function of z and t, and if we assume a planar invariance (no dependence in x and y), it is given by the 1D diffusion dynamics,

$$\partial_t w_{\mathrm{XOH}} = \kappa\, \partial_{z^2} w_{\mathrm{XOH}}, \tag{3}$$

where κ is the XOH diffusion coefficient. The boundary conditions for the film evolution and for the XOH mass balance are crucial in the w_{XOH} evolution. Indeed, as water evaporates at the interface $z = h(t)$, XOH concentrates there (since the XOH does not evaporate at this time scale), and this high concentration diffuses within the film. This process can be described by the following boundary conditions:

$$\dot{h} = \frac{dh}{dt} = \mathcal{F}(h(t)), \tag{4}$$

with

$$\partial_z w_{\mathrm{XOH}}(0,t) = 0; \quad \kappa \partial_z w_{\mathrm{XOH}}(h(t),t) = -\dot{h} w_{\mathrm{XOH}}(h(t),t) \tag{5}$$

for the XOH concentration at $z = 0$ (no flux) and $z = h(t)$. If the diffusion coefficient κ is constant, this system of equations is linear in the mass fraction. Moreover, this model is consistent with previous models used for pure fluids [2]. Modeling the diffusion coefficient is difficult since it should be a complex function of the polymer matrix, temperature, and humidity rate, in particular. However, some simple assumptions can explain most of the droplet formation mechanism. First, since the evaporation rate is almost constant over the time range where the droplets appear, we consider a constant evaporation rate. We can extract the diffusion coefficient κ from the experiments by assuming that the droplets appear when w_{XOH} reaches 2.4% at one position in the film. Fitting κ for each experiment using this criterion, we obtain $\kappa = 0.17 \pm 0.03\ \mu\mathrm{m}^2\,\mathrm{s}^{-1}$, showing that this approach is consistent. Finally, using this value

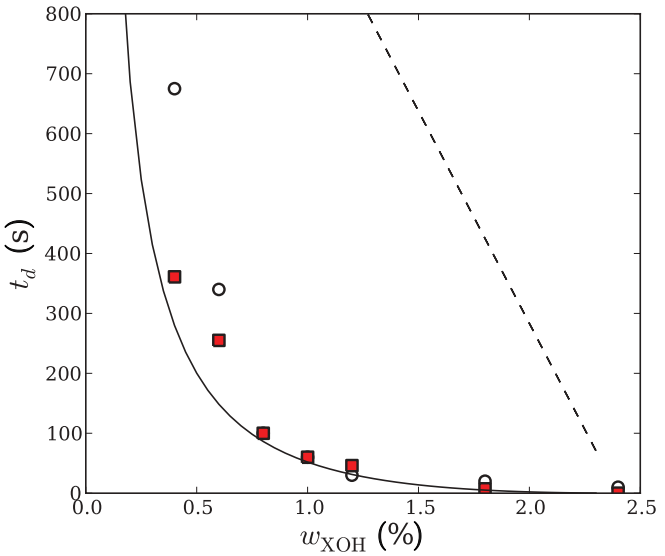

FIG. 6. (Color online) Time of droplet formation as a function of w_{XOH}. The circles: data are in good agreement with the solid line: diffusion model as opposed to a dashed line: simple dilution model. The squares show the time of formation calculated with the diffusion model but using the measured evaporation rate for each case.

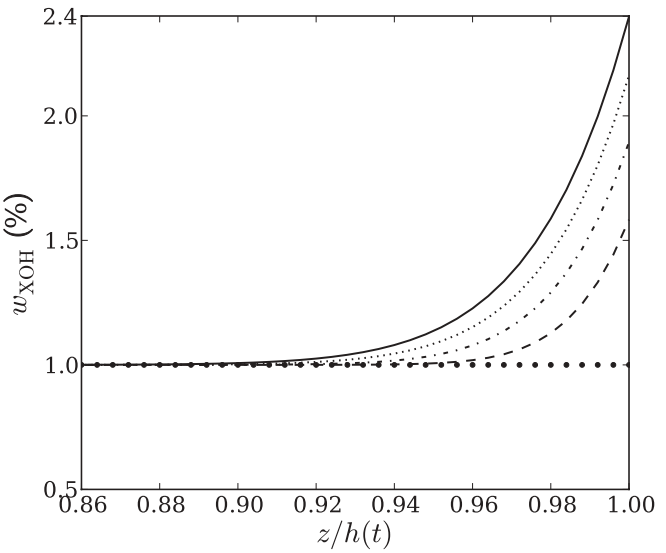

FIG. 7. The XOH mass fraction profiles near the interface for different times ($t = 0$, 13, 26, 39, and 52 s for increasing curves, respectively). The profiles are scaled vertically by the film height $h(t)$ so that the interface is always located at $z/h(t) = 1$.

of κ, we numerically can reversely compute the time of droplet apparition for any initial concentration of XOH, and good agreement is found between the data and the model (Fig. 6). Figure 7 shows the mass fraction profiles of XOH near the interface for the film with an initial concentration of $w_{\mathrm{XOH}} = 1\%$. It illustrates the accumulation of XOH near the interface where it crosses the miscibility limit.

Finally, this model can be improved by taking the measured evaporation rate for each measurement instead of the constant rate approximation, represented by the squares in Fig. 6. For initial w_{XOH} above 0.8%, this model shows no significant difference with the experiments. However, the diffusion model, either with the constant evaporation rate or by taking the measured evaporation rates, is less accurate for low initial w_{XOH}, probably because the mixture becomes highly concentrated in the polymer when the demixing transition occurs, changing, for instance, the miscibility limit.

IV. DISCUSSION

Our results suggest a different type of scenario for the formation of droplets and craters observed on the surface of the dried films in contrast with recent papers where structured interfaces where obtained through water droplet condensation [17] or thermocapillary convection [20]. After the film is spread, the water begins to evaporate, leading to a decrease in the film thickness [Fig. 8(a)]. At time t_d, droplets are formed by the demixing transition into a zone rich in XOH, close to the interface. As the evaporation proceeds, the film thickness decreases further, its viscosity increases, and droplets subjected to mechanical pressures imposed by the film are trapped and are distorted with some flattening. When the film no longer contains significant water, droplets appear at its surface [Figs. 8(b) and 8(c)]. The water contained in the droplets is trapped by the XOH, whose saturated vapor pressure is very low. When the film has almost completely dried, it imposes a high mechanical pressure that bursts the droplets, liberating their water. After total evaporation, craters are left on the rigid film. Therefore, at time t_f, once the film has completely dried, several craters can be seen, reflecting the outline of the dried droplets [Fig. 8(d)]. It is not clear yet whether the observed craters are bad or good for cosmetic applications, suggesting future research directions: On one hand, they increase the apparent roughness of the skin, but, on the other hand, they might enhance the film porosity and, thus, allow the skin to breathe.

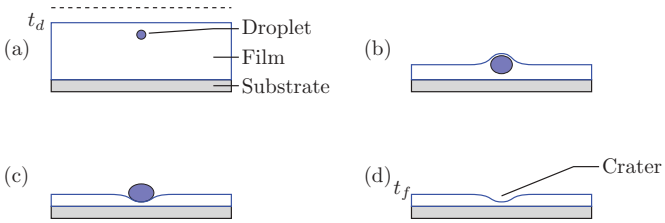

FIG. 8. (Color online) Schematic evolution of the droplets to craters. (a) Formation of droplets in the film very close to the free surface. The dashed line indicates the initial level of the film; (b) growth of the drops by coalescence; (c) leveling of the droplets at the surface; (d) formation of the craters.

V. CONCLUSION

Following *in situ* thin film evaporation of a formulation composed of essentially water, polymer, and alcohol, we have characterized the dehydration process under well-controlled physical conditions: constant temperature, constant relative humidity, and uniform film thickness. The experimental observation and characterization of the formation of droplets, leading to craters as the film dries in about 30 min, were interpreted using a numerical approach. We have shown, by a simple physical model, that the droplets appear when the alcohol locally exceeds its partial miscibility, showing that a constituent—even at very low concentration—can have a considerable effect on the topography of a dried polymer film on the microscopic scale. It follows that the formation of droplets and craters is closely linked to the physicochemical properties specific to the alcohol, i.e., partial miscibility in water, low saturated vapor pressure, dynamic viscosity, and surface tension. Our results show that it is possible to select a specifically tailored alcohol with suitable physicochemical properties in order to control the formation of craters.

The resulting uneven topography has a significant repercussion on the film's properties, in particular, its porosity and elasticity. If the diameter and depth of the craters could be manipulated, for instance, by varying the initial XOH mass fraction, the mechanical properties of the film (microporosity, patterned surface, microencapsulation, etc.) could be tailored for specific applications. We are expanding this paper and are examining the impact of the substrate on the physics of the dehydration process, in particular, the influence of the porosity and the curvature of the substrate.

[1] J. Vrentas and C. Vrentas, J. Polym. Sci. **32**, 187 (1994).
[2] R. D. Deegan, O. Bakajin, T. F. Dupont, G. Huber, S. R. Nagel, and T. A. Witten, Nature (London) **389**, 827 (1997).
[3] D. Urban and K. Takamura, *Polymer Dispersions and Their Industrial Applications* (Wiley-VCH, Weinheim, 2005).
[4] Y. Xie and R. H. Friend, Appl. Phys. Lett. **88**, 163508 (2006).
[5] G. Gauthier, V. Lazarus, and L. Pauchard, Langmuir **23**, 4715 (2007).
[6] E. R. Dufresne, E. I. Corwin, N. A. Greenblatt, J. Ashmore, D. Y. Wang, A. D. Dinsmore, J. X. Cheng, X. S. Xie, J. W. Hutchinson, and D. A. Weitz, Phys. Rev. Lett. **91**, 224501 (2003).
[7] E. R. Dufresne, D. J. Stark, N. A. Greenblatt, J. X. Cheng, J. W. Hutchinson, L. Mahadevan, and D. A. Weitz, Langmuir **22**, 7144 (2006).
[8] D. J. Harris, H. Hu, J. C. Conrad, and J. A. Lewis, Phys. Rev. Lett. **98**, 148301 (2007).

[9] G. Berteloot, C.-T. Pham, A. Daerr, F. Lequeux, and L. Limat, Europhys. Lett. **83**, 14003 (2008).
[10] C. Parneix, P. Vandoolaeghe, V. S. Nikolayev, D. Quéré, J. Li, and B. Cabane, Phys. Rev. Lett. **105**, 266103 (2010).
[11] R. D. Deegan, Phys. Rev. E **61**, 475 (2000).
[12] Y. O. Popov and T. A. Witten, Phys. Rev. E **68**, 036306 (2003).
[13] P. G. de Gennes, Rev. Mod. Phys. **57**, 827 (1985).
[14] F. Ziebert and E. Raphaël, EPL **86**, 46001 (2009).
[15] G. Jing, H. Bodiguel, F. Doumenc, E. Sultan, and B. Guerrier, Langmuir **26**, 2288 (2010).
[16] L. Pauchard, Europhys. Lett. **74**, 188 (2006).
[17] A. Böker *et al.*, Nat. Mater. **3**, 302 (2004).
[18] H. Matsuyama, M. Teramoto, R. Nakatani, and T. Maki, J. Appl. Polym. Sci. **74**, 159 (1999).
[19] M. Yamamura, T. Nishio, T. Kajiwara, and K. Adachi, Chem. Eng. Sci. **57**, 2901 (2002).
[20] M. Srinivasaro, D. Collings, A. Philips, and S. Patel, Science **292**, 79 (2001).
[21] B. Cabane and S. Henon, *Liquides; Solutions, Dispersions, Emulsions, Gels (in French)* (Belin, Paris, 2003).
[22] F. Doumenc, B. Guerrier, and C. Allain, Europhys. Lett. **76**, 4 (2006).
[23] M. Yoshida and H. Miyashita, Chem. Eng. J. **86**, 193 (2002).
[24] R. D. Deegan, O. Bakajin, T. F. Dupont, G. Huber, S. R. Nagel, and T. A. Witten, Phys. Rev. E **62**, 756 (2000).
[25] X. Xu and J. Luo, Appl. Phys. Lett. **91**, 124102 (2007).
[26] J. Li, B. Cabane, M. Sztucki, J. Gummel, and L. Goehring, Langmuir **28**, 200 (2012).
[27] N. Shahidzadeh-Bonn, S. Rafaï, A. Azouni, and D. Bonn, J. Fluid Mech. **549**, 307 (2006).
[28] B. Guerrier, C. Bouchard, C. Allain, and C. Bénard, AIChE **44**, 791 (1998).
[29] A. F. Routh and W. B. Zimmerman, Chem. Eng. Sci. **59**, 2961 (2004).